PLOS ONE

RESEARCH ARTICLE

Rapid and sensitive detection of selective 1,2-diaminobenzene based on facile hydrothermally prepared doped Co_3O_4/Yb_2O_3 nanoparticles

Mohammed M. Rahman *

Department of Chemistry, King Abdulaziz University, Faculty of Science, Jeddah, Saudi Arabia

* mmrahman@kau.edu.sa, mmrahmanh@gmail.com

Abstract

In this approach, the performance of a newly developed sensor probe coated with low-dimensional Co_3O_4/Yb_2O_3 nanoparticles (NPs) in rapidly detecting 1,2-diaminobenzene was evaluated by an electrochemical technique. The sensor probe was fabricated by depositing a very thin layer consisting of synthesized Co_3O_4/Yb_2O_3 NPs using a 5% Nafion conducting binder onto a glassy carbon electrode (GCE). The facile hydrothermally prepared Co_3O_4/Yb_2O_3 NPs were totally characterized by conventional methods such as FTIR, UV-vis, TEM, XPS, EDS, and XRD analyses. The fabricated chemical sensor probe was found to exhibit long-term activity, stability in electrochemical response, good sensitivity (5.6962 $\mu A \mu M^{-1} cm^{-2}$), lowest detection limit (0.02±0.001 pM), and broad linear dynamic range (0.1 pM to 0.01 mM). The observed performances suggest that the newly introduced sensor could play an efficient role in detecting 1,2-diaminobenzene especially in healthcare and environmental applications on a broad scale.

Introduction

Generally, 1,2-diamino benzene (1,2-DAB) is an organic amine and industrially very important chemical intermediate. It has extensive usage in producing medicine, auxiliaries, pesticides, dyes, pigments, photosensitive materials and, so on [1]. 1,2-DAB has also been reported [2, 3] as a carcinogenic and mutagenic substance causing hazardous effects in the human body through inhalation, ingestion, eye contact and, so on. Heavy exposure to1,2-DAB can often cause cancer and damage liver, respiratory, and digestive systems of the human body. The ACGIH (American Conference of Governmental Industrial Hygienists) has identified 1,2-DAB as a serious hazardous substance that causes environmental pollution [4]. Therefore, it drives the need to search for a sustainable method to detect 1,2-DAB efficiently. Currently, various numerical methods including liquid chromatography [5–7], spectrophotometry [8, 9], capillary electrolysis [10], etc are widely used in detecting 1,2-DAB. The technical advantages of these methods include good sensitivity, high selectivity, and long-term stability. However, these approaches have different drawbacks including complicated detection process,

Competing interests: The authors have declared that no competing interests exist

specialized instrumentation, laborious, high cost, and so on [11]. To ensure the real-time detection of this hazardous toxin, the electrochemical method is most effective. Due to the attractive electrical and optical properties, the various nanostructured metal oxides such as Pd-Rh nano-frames [12], Au@Pt core/shell nanorods [13], Fe_3O_4 magnetic nanoparticles [14], and tungsten carbide nanorods [15] have been recognized as potential sensing elements in the chemical sensor for detecting 1,2-DAB. The chemical sensor fabricated by Fe_3O_4 doped functionalized multiwall carbon nanotubes composite (Fe_3O_4@f-MWCTNs) is reported for its efficient performance with the sensitivity of 2.8002 $mAmM^{-1}cm^{-2}$ as well as the detection limit of 50.0 μM [16]. Similarly, Fe-MIL-88-H_2O_2-OPD based DAB (diaminobenzene) chemical is reported for its good performance with 50.0 nM– 30.0 μM LDR and 46.0 nM DL [17].

In the present study, Co_3O_4/Yb_2O_3 NPs/Binder/GCE based on a novel electrochemical sensor is introduced for detecting 1,2-DAB in an optimized buffer system successfully. Firstly, the slurry of Co_3O_4/Yb_2O_3 NPs in ethanol is prepared and then deposited a very thin layer onto GCE with an additive of 5% Nafion binder. This fabricated sensor is applied to detect selective 1,2 DAB through the implementation of a reliable electrochemical method by using the electrochemical approach. It is worth mentioning that the development of Co_3O_4/Yb_2O_3 NPs based GCE sensor seems to be promising technology especially for detecting toxicant to the safety of the environment.

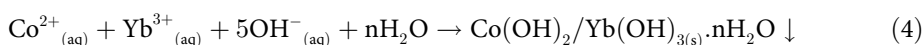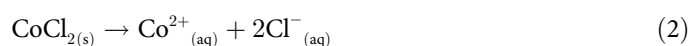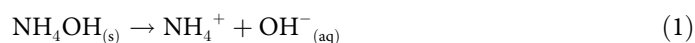## Experimental procedures

Materials and experimental methods

The required inorganic salts of cobalt (II) chloride ($CoCl_2$), ytterbium chloride ($YbCl_3$) and ammonium hydroxide (NH_4OH) for preparing the required nano-materials supplied by SAC (Sigma Aldrich Company), USA. The other required ingredients including analytical grade 1,2-diamino benzene (1,2-DAB), 3-methyl aniline (3-MA), 3-chlorophenol (3-CP), 2,4-dinitrophenol (2,4-DNP) benzaldehyde (BH), pyridine (P), 3-methoxy hydrazine (3-MPHyd), ammonium hydroxide (AH), ethanol (E), tetrahydrofuran (3-THF), 5% Nafion, monosodium phosphate ($NaHPO_4$) and disodium phosphate (Na_2PO_4) were also purchased from the Sigma Aldrich Company. The prepared NPs were analyzed by XRD for identifying its crystalline phases. FESEM (JSM7600F, JEOL, Japan) was used to investigate elemental analysis, molecular arrangement, shape and size as well as morphological structure. The XPS (Thermo scientific, K-α1 1066) analysis was conducted to examine the binding energy among Co, Yb, O and their states of oxidation. The details of the XPS excitation radiation source are as follow: Al K-α1, 300.0 μm beam spot, 200.0 eV pass energy, 10^{-8} Torr pressure. The prepared Co_3O_4/Yb_2O_3 NPs were also examined by UV-vis spectrophotometer and FTIR (Thermo scientific NICOLET iS50, Madsion, USA). During fabricating the chemical sensor probe, an ethanolic slurry of calcined Co_3O_4/Yb_2O_3 NPs and 5% Nafion were used to develop a thin layer on GCE. It was then employed for detecting 1,2-DAB in aqueous medium. The Keithley electrometer (6517A; Purchased from the USA) was utilized to conduct electrochemical analysis through electrochemical technique.

Hydrothermal process to prepare Co_3O_4/Yb_2O_3 NPs

The facile hydrothermal process is applied to prepare the Co_3O_4/Yb_2O_3 NPs. The hydrothermal is an efficiently used method to synthesis nano-doped material. This process basically consists of three major steps. These include (i) hydroxides co-preparation in aqueous medium, (ii) precipitation drying, and then (iii) calcining in the muffle furnace. For executing the experimentation, ytterbium chloride ($YbCl_3$) and cobalt chloride ($CoCl_2$) are dissolved in 100.0 mL de-ionized water. This mixing process is done in 250.0 mL conical flask. Since the

hydrothermal process works in an alkaline medium, 0.1 M NH_4OH solution is added dropwise for adjusting the pH at 10.5 under continuous magnetic stirring. The ions Co^{+2} and Yb^{+3} are co-precipitated with the state of $Co(OH)_2/Yb_3(OH)_2$. The formed metal hydroxides are separated and then carefully washed with di-ionized water as well as ethanol. Then the separated precipitate is dried in an oven at a temperature of 105 ˚C. Subsequently, the dried precipitate is placed inside the furnace to calcine at 500 ˚C temperature for 6h. In the presence of oxygen, this calcination process transforms the metal hydroxides into Co_3O_4/Yb_2O_3 NPs. The obtained sample is then ground to particles at nano level by using a motor. The possible reaction schemes are listed below:

Reactions in aqueous medium

$$NH_4OH_{(s)} \rightarrow NH_4^+ + OH^-_{(aq)} \tag{1}$$

$$CoCl_{2(s)} \rightarrow Co^{2+}_{(aq)} + 2Cl^-_{(aq)} \tag{2}$$

$$YbCl_{3(s)} \rightarrow Yb^{3+}_{(aq)} + 3Cl^-_{(aq)} \tag{3}$$

$$Co^{2+}_{(aq)} + Yb^{3+}_{(aq)} + 5OH^-_{(aq)} + nH_2O \rightarrow Co(OH)_2/Yb(OH)_{3(s)}.nH_2O \downarrow \tag{4}$$

Reactions occurred in muffle furnace

$$Co(OH)_2/Yb(OH)_{3(s)} + O_2 \rightarrow Co_3O_4/Yb_2O_3 + H_2O_{(v)} \tag{5}$$
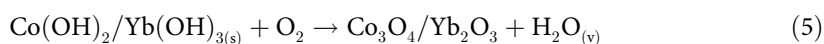
Due to the presence of several metal ions in the reaction medium, the precipitation of metal ions as metal hydroxides are dependent on the product solubility (Ks) of the corresponding metal hydroxides. It is noted that the values of product solubility (Ks) for $Yb(OH)_3$ and Co $(OH)_3$ are 1.0×10^{-22} and 5.92×10^{-15} respectively [18]. As the addition of 0.1 M NH_4OH solution dropwise in the reaction medium, the concentration of OH^- is increased gradually. Therefore, $Yb(OH)_3$ starts to precipitate first due to its lower value of product solubility (Ks). It forms Yb $(OH)_3$ crystal nuclei and then starts the aggregation. However, as the pH keeps increasing, the $Co(OH)_3$ starts precipitating at a certain pH value. These precipitations are then absorbed on crystallites of $Yb(OH)_3$. Similar growth patterns of nano-materials are reported in literature [19–21]. The calcined Co_3O_4/Yb_2O_3 NP is then ground in a mortar to make a powder sample for full of characterization. The prepared Co_3O_4/Yb_2O_3 NPs are applied to detect the selective 1,2-DAB through an electrochemical approach at room temperature.

GCE fabrication by using Co_3O_4/Yb_2O_3 NPs

A slurry/paste of Co_3O_4/Yb_2O_3 NPs was prepared by mixing ethanol in order to prepare a thin layer coated GCE. The prepared GCE was then dried at ambient temperature. A drop of 5% ethanolic emulsion of Nafion (so-called conducting binder) was added during the coating process to enhance the binding strength between GCE and used NPs. It is worth mentioning that Nafion has been reported in the literature for its capability to improve conductivity, stability, and electron transfer rate of the electrode [22, 23]. For drying the produced conducting film entirely, the fabricated electrode was put inside an oven at 34.0 ˚C temperature. At the next stage, the prepared Co_3O_4/Yb_2O_3 NPs/binder/GCE and 1.5 mm dia Pt-wire were used as working and counter electrode respectively for making an electrochemical cell. The 1,2-DAB

solution was used as a target analyte in the developed chemical sensor. The sensitivity (Sen) of the sensor was determined from the calibration curve that represents current vs. concentrations. Similarly, DL and LDR were determined from noise and sensitivity. The used Keithley electrometer (6517A, USA) consisting of two electrode systems supplies voltage in developing electrochemical curve. Throughout this chemical experimentation, the solution with 0.1 PBS was kept constant to 10.0 mL in glass beakers.

Results and discussions

Analysis of structural and optical properties

The obtained FT-IR spectra of Co_3O_4/Yb_2O_3 NPs are presented in Fig 1A. The FT-IR spectrum of Co_3O_4/Yb_2O_3 NPs is displayed two distinctive peaks at 552 and 654 cm^{-1}, which originate from metal-oxygen stretching vibration. The bands at 552 and 654 cm^{-1} are associated with Co^{+3}-O and Co^{+2}-O vibration respectively [24, 25]. The adsorption peaks at wavenumber 1407, 1625, and 3306 cm^{-1} are more likely attributed to the stretching vibration mode of O-H due to the adsorption of water from the environment [26–28]. The photo-electronic sensitivity through UV-vis analysis of prepared Co_3O_4/Yb_2O_3 NPs was conducted at 290–800 nm wavelength. Due to the adsorption of visible light radiant energy, the electrons of synthesized NPs are transmitted from the low-level to high-level, which resulted in UV-vis spectra [29]. The
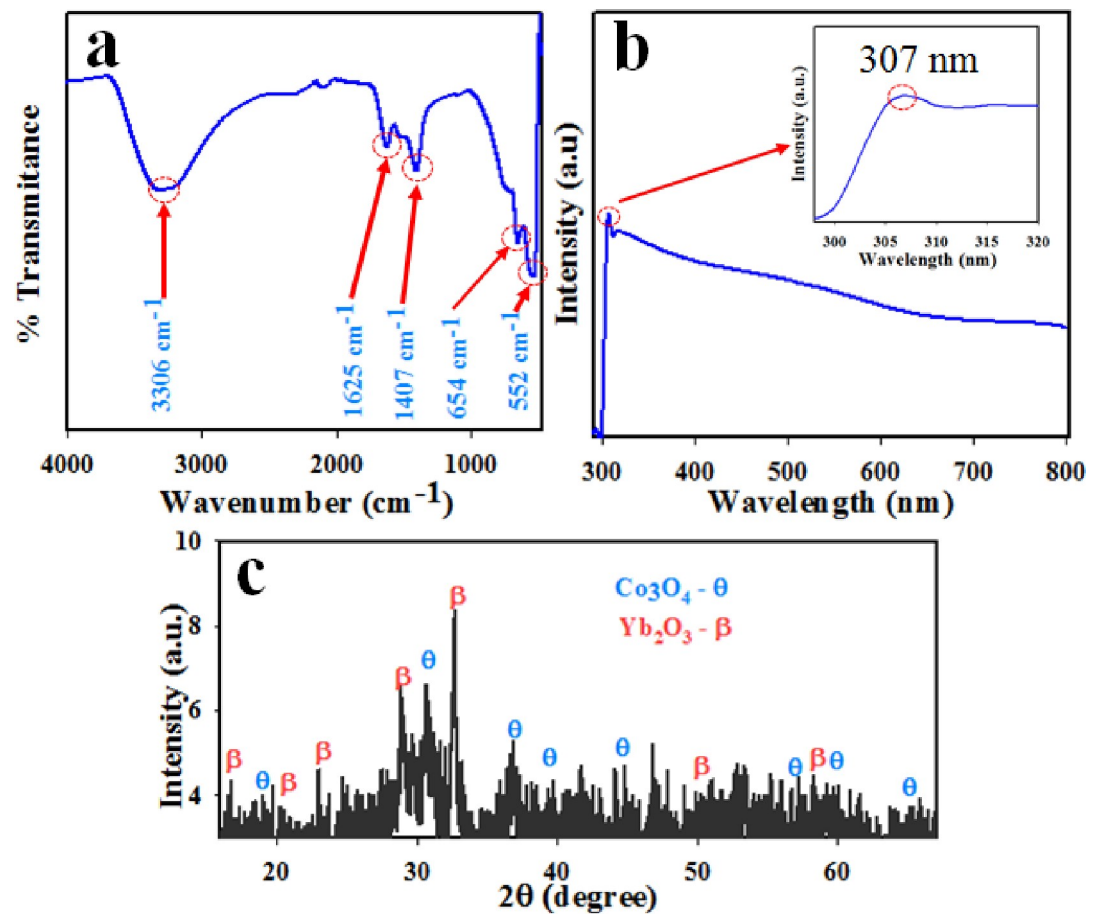

Fig 1. (a) FT-IR, (b) UV-vis spectrum, and (c) XRD patterns of Co_3O_4/Yb_2O_3 NPs for evaluation of optical and morphological properties.
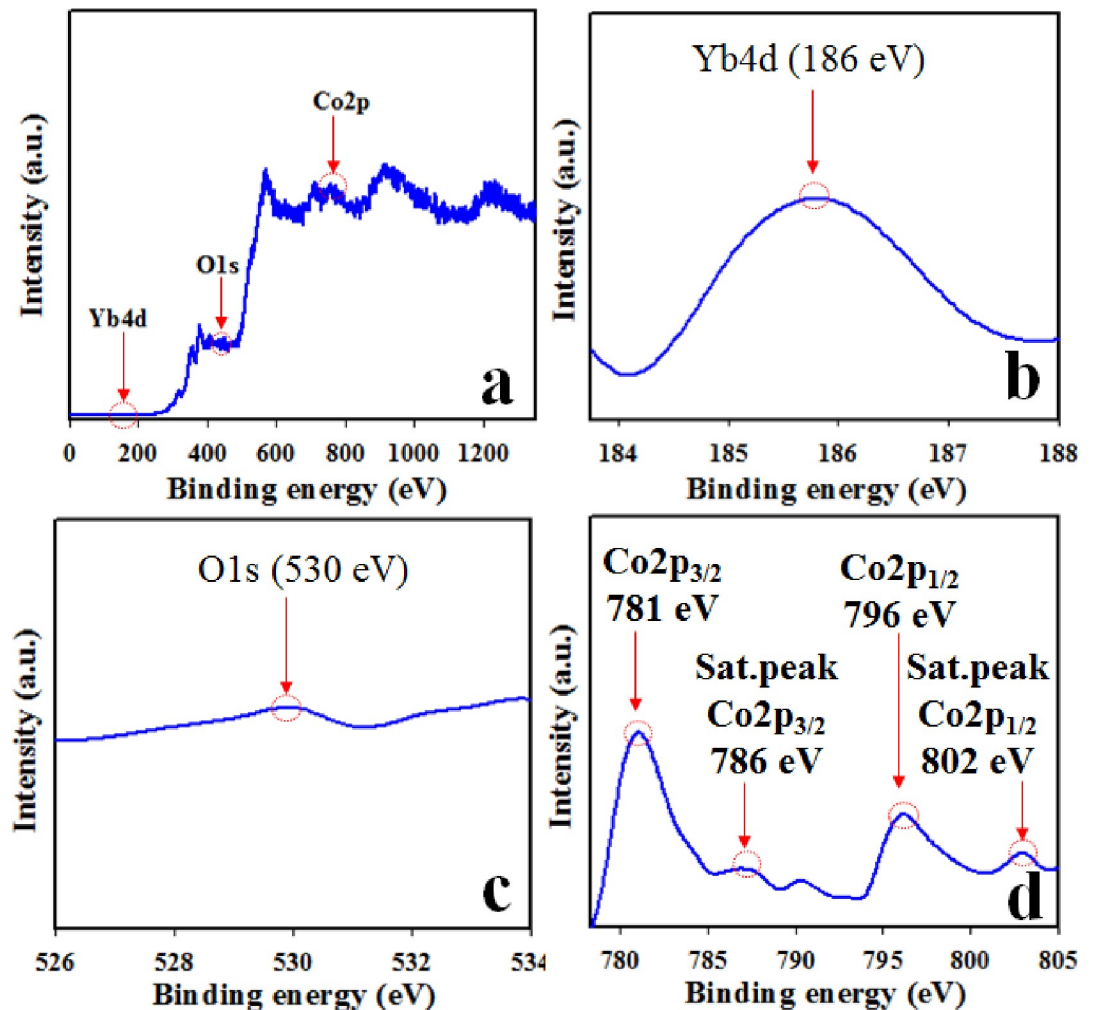
Fig 2. XPS analysis of Co_3O_4/Yb_2O_3 NPs: (a) Full range spectrum; Orbital spins of (b) Yb4d-level, (c) O1s-level, and (d) Co2p-level.

typical UV-vis spectra are presented in Fig 1B. An intense peak (as shown in the inset, Fig 1B) is observed at 307.0 nm. This could be the characteristic bond of synthesized Co_3O_4/Al_2O_3 NPs. The obtained UV absorption band is in good agreement with the literature [30–32]. As per Eq (6), the measured band-gap energy is found to be 4.04 eV.

$$E_g = 1240/\lambda_{max} \tag{6}$$

Where, E_g: band-gap energy; λ_{max}: maximum absorbed wavelength [33, 34].

The X-ray diffraction (XRD) analysis was conducted on Co_3O_4/Yb_2O_3 NPs in the range of 10 to 80 degrees at the scanning speed of 2 / min. The obtained XRD spectrum is presented in Fig 1C which shows the well-crystalline phases of Co_3O_4 and Yb_2O_3. The reflected crystalline peaks of Co_3O_4 indices as θ are (111), (220), (311), (400), (420), (440), and (511) as identified in the literature [35–37] accordingly JCPDS 42–1467. Moreover, the identified peaks of Yb_2O_3 indices as ß are (200), (211), (220), (222), (400), (440) and (622) as reported by the studies [38, 39] accordingly JCPDS No. 87–2374.

As per general practice, the crystal size of synthesized NPs is measured from XRD diffraction patterns by using Eq (7).

$$D = 0.91\ \lambda/(\beta\ \cos\theta) \tag{7}$$

Here, λ: wavelength, β: width at half corresponding to the highest intense peak, and θ: diffraction angle [40]. The measured crystal size by using Eq (7) is found to be 27.03 nm.

Analysis of binding energy

The prepared NPs of Co_3O_4/Yb_2O_3 were also analyzed by the XPS technique. When Co_3O_4/Yb_2O_3 NPs are scanned using XPS, the valence electron from outer orbit transmits from low-energy level to high-energy level owing to the kinetic energy of the X-ray beam absorbed. This practice is utilized to determine the atomic composition as well as oxidation compounds present in the tested sample [41–43]. The obtained XPS spectra are presented in Fig 2A for Co2p, Yb4d, and O1s. The Co2p core level spectrum presented in Fig 2D shows two dominating peaks of Co2p3/2 and Co2p1/2 at 781 eV and 796 eV respectively along with satellite peaks. These two dominating sharp peaks can be recognized to verify the existence of Co^{+3}. The observed satellite peaks of Co2p3/2 and Co2p1/2 are at 786 eV and 802 eV respectively. These two peaks are more likely ascribed to the presence of Co^{+2} in the prepared Co_3O_4/Yb_2O_3 NPs [44–48]. Thus, the presence of Co2p spin orbitals demonstrates the co-existence of Co(II) and Co(III) on the synthesized Co_3O_4/Yb_2O_3 NPs. The O1s peak at 530 eV as shown in Fig 3C is
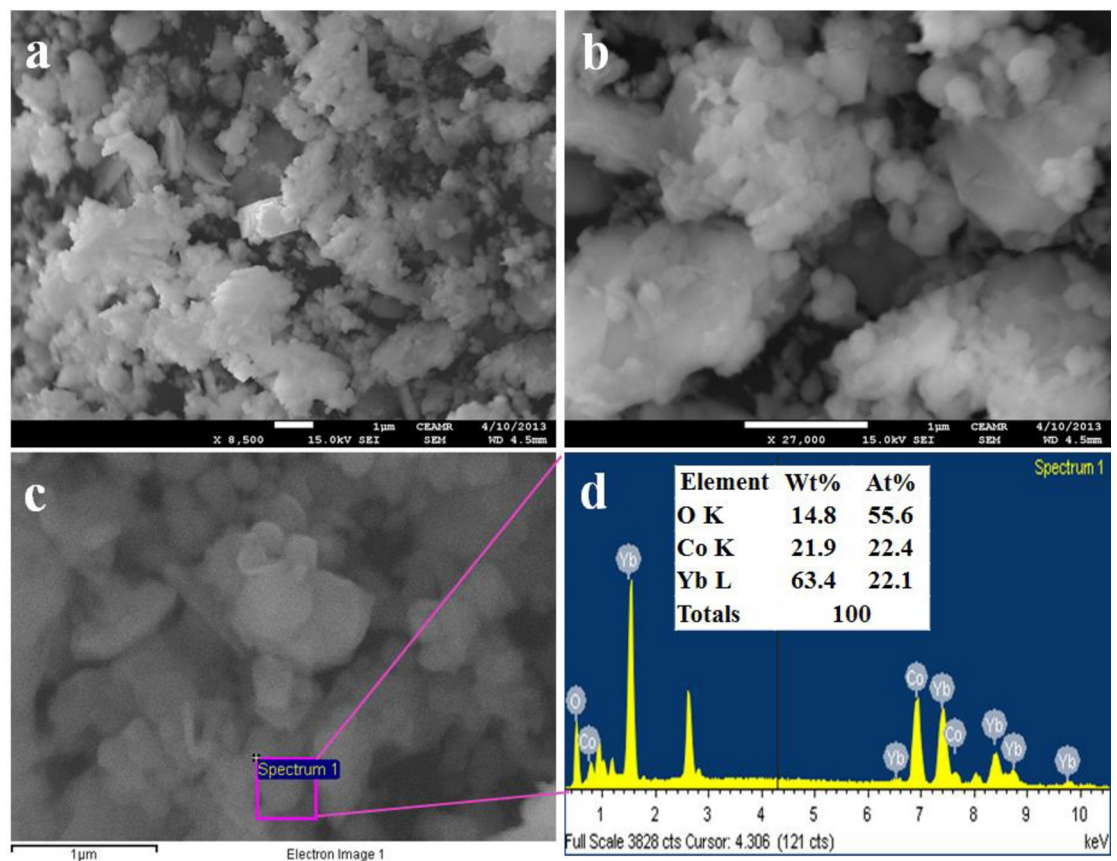

**Fig 3. Morphology and elemental analyses.** (a-b) FESEM micrographs, (c-d) EDS analysis of Co_3O_4/Yb_2O_3NPs.

attributed to the O^{2-} in Co_3O_4 [49–51]. Similarly, the Yb4d peak at 186 as is ascribed to Yb^{+3} – O^{-2} bonds in Yb_2O_3 as illustrated in Fig 3B [52–54].

Elemental and morphological analysis

Fig 3 represents the morphological and elemental analysis of prepared NPs of Co_3O_4/Yb_2O_3 and this analysis was carried out by the implementation of FESEM and EDS on the synthesized sample. Fig 3A and 3B clearly shows that the prepared Co_3O_4/Yb_2O_3 nanomaterials are spherical in shape [55–57]. The elemental analysis of Co_3O_4/Yb_2O_3 NPs as per EDS test presented in Fig 2C and 2D shows O 14.8%, Yb 63.4%, and Co 21.9%. Besides this, there is no other visible peak and therefore it can be concluded that the prepared Co_3O_4/Yb_2O_3 NPs consist of cobalt, ytterbium, and oxygen only [58, 59].

Applications: Detection of 1,2-DAB by Co_3O_4/Yb_2O_3 NPs

The conductive binder (5% Nafion) was used during the fabrication of the sensor probe through the deposition of a thin layer of Co_3O_4/Yb_2O_3 NPs on GCE. The use of conductive binder successfully improved its conductivity, stability, and electron transfer rate. The prepared Co_3O_4/Yb_2O_3NPs/binder/GCE based chemical sensor was then employed to detect 1,2-DAB selectively in optimized aqueous buffer solution. In electrochemical detection of 1,2-DAB by electrochemical method, current versus potential was determined on the thin film of Co_3O_4/Yb_2O_3 NPs by fixing the holding time for 1 s. Scheme 1 presents the possible reaction mechanism of 1,2 DAB. It is worth mentioning that enrichment of electrons is observed during the determination of sensing performance. Thus, the conductivity of the sensing medium of 1,2-DAB is increased. As a result, amplified electrochemical responses as illustrated in Fig 5A are found to be significant with the increment of 1,2-DAB concentration. It seems that the reactive 1,2-DAB is absorbed on the fabricated working electrode (GCE coated of $Co_3O_4/$
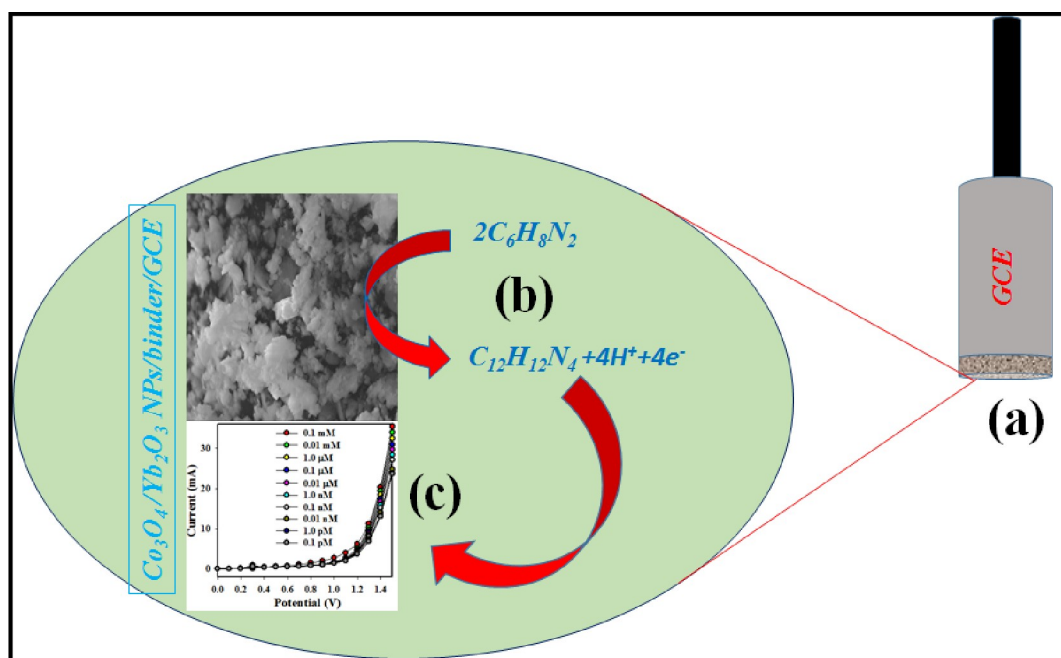
Scheme 1. Schematic representation of the possible detection mechanism of target 1,2-DAB onto Co_3O_4/Yb_2O_3 NPs/ Nafion/GCE.
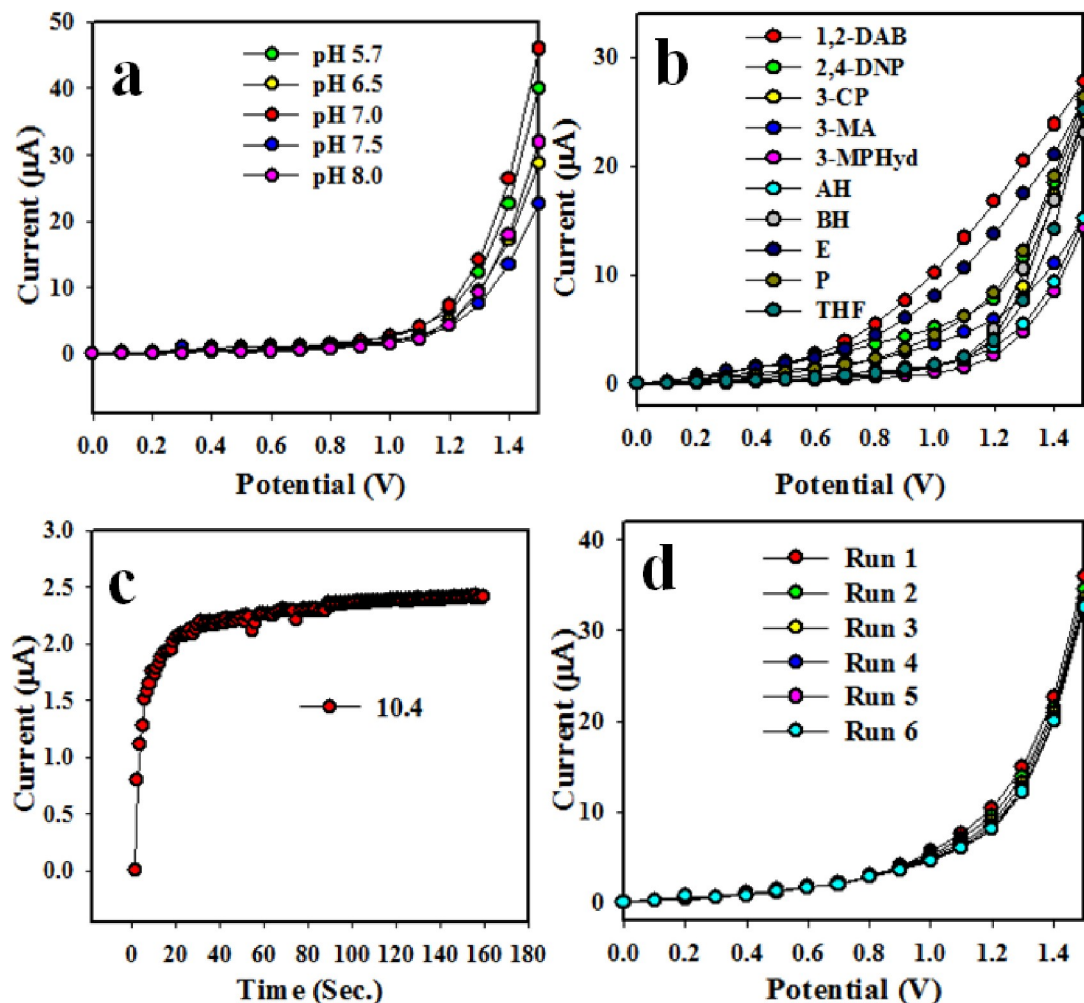
Fig 4. Optimization of Co_3O_4/Yb_2O_3 NPs/binder/GCE based 1,2-DAB chemical sensor: (a) optimization of pH, (b) level of selectivity, (c) response time and (d) degree of repeatability.

Yb_2O_3 NPs) surface as per reaction (8) and consequently the oxidation reactions are started. The produced electrons and hydrogen ions from oxidation of 1,2-DAB as shown in reaction (8) effectively increase the conductivity of the sensing medium [16, 60, 61]. This is why the electrochemical responses are observed to be more significant with the increase of 1,2-DAB concentrations. This demonstrates that the electrochemical responses are directly proportional to the concentration of 1,2-DAB. This is in good agreement with the results reported elsewhere [62]. The pictorial representation of the Co_3O_4/Yb_2O_3 NPs modified electrode in detecting of 1,2-DAB is demonstrated in Scheme 1.

The possible oxidation reaction of 1,2-DAB is presented by reaction (8) below.

$$2C_6H_8N_2 \rightarrow C_{12}H_{12}N_4 + 4H^+ + 4e^- \qquad (8)$$
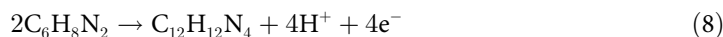
The hydrothermally prepared Co_3O_4/Yb_2O_3 NPs are not similarly active to all the phosphate buffer systems in applied electrochemical method. Therefore, it is very important to optimize the buffer solution for obtaining the maximum electrochemical responses. The fabricated Co_3O_4/Yb_2O_3 NPs/binder/GCE based sensor probe was examined in different buffer solutions with pH ranging from 5.7 to 8.0 The tested chemical sensor probe was maximum
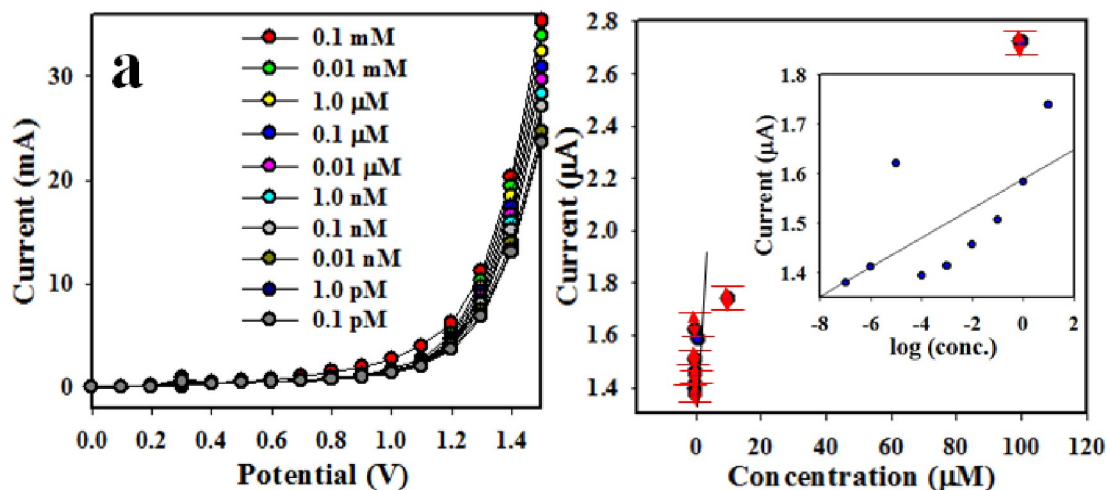
Fig 5. (a) Effect of concentration variation on the performance of Co_3O_4/Yb_2O_3 NPs/binder/GCE based 1,2-DAB chemical sensor through (a) I-V graphical presentation, (b) current versus concentration curve (Inset: Log [Conc. Of 1,2-DAB] versus current).

current at pH of 7 as it is shown in Fig 4A. This performance (pH optimization) test was conducted by using Keithley electrometer at applied potential range 0–1.5 V. The electrochemical responses were recorded for different concentrations ranging from 1.0 nM of 1,2-DAB and pH of 7. Such responses of 1,2-diamino benzene (1,2-DAB), 2,4-dinitro-phenol (2,4-DNP) 3-methyl aniline (3-MA), benzaldehyde (BH), 3-methoxy phenyl hydrazine (3-MPHyd), 3-chlorophenol (3-CP), pyridine (P), ammonium hydroxide (AH), ethanol (E) and tetrahydro-furan (THF) are illustrated in Fig 4B. Among others, 1,2-DAB was found to exhibit the maximum electrochemical responses. The key analytical performance of a sensor is denoted by the response time. This test was conducted in 1.0 nM concentration for 1,2-DAB to optimize in buffer solution. The highly applicable value of the response time as per observation from Fig 4C is 11.0 sec. Reproducibility is another important sensor performance parameter. The data on reproducibility is presented in Fig 4D after conducting the test in 1.0 nM concentration of 1,2-DAB and pH of 7. The responses were observed to be outstanding even after washing the working electrode in each trail. At the next stage, RSD (relative standard deviation) was calculated. It was found to be 2.26 at +.8 V potential.

Fig 5 shows the graphical presentation of current versus the potential for 1,2-DAB detection at the concentration ranging from 0.1 mM to 0.1 mM. The observed responses corresponding to the concentration are found to be distinguishable. The resulted plot shows the regression coefficient value (r^2 = 0.9745) at +1.0 V potential. The estimated sensitivity and LDR (Linear dynamic range) are found to be 5.6962 $\mu A \mu M^{-1} cm^{-2}$ and 0.1 pM– 0.01 mM respectively. The detection limit (DL) is calculated as 0.02 ± 0.001 pM (signal to noise ratio of 3).

Fig 5A demonstrates that the electrochemical response varies with the concentration of 1,2-DAB which is in good agreement with the finding reported in the literatures [63–65]. A few 1,2-DAB chemicals are absorbed in the very beginning of the sensing performance of 1,2-DAB with the Co_3O_4/Yb_2O_3 NPs/binder/GCE sensor probe. The absorption of 1,2-DAB mainly occurs when oxidation starts progressively onto the working electrode surfaces [66]. In the meantime, the analyte concentration on the surface increases and covers a larger part of the surface. It indicates a gradual increase of reaction rate on the Co_3O_4/Yb_2O_3 NPs/binder/GCE surface. However, the surface reaction rate and corresponding current density reach a

Table 1. The comparative performances of different chemical sensors in detecting 1,2-DAB based on various electrode modification.

Modified electrode system	Detection limit (DR)	Linear dynamic range (LDR)	Sensitivity	Ref.
Fe_3O_4@f-MWCNTs	50.00 μM	0.6–80 μM	2.80 $\mu A\mu M^{-1}cm^{-2}$	[16]
Co_3O_4/Yb_2O_3 NPs /GCE	0.02 pM	0.1 pM ~0.01 mM	5.69 $\mu A\mu M^{-1}cm^{-2}$	This work

*nM–Nanomole, μM–Micromole, pM–picomole.

https://doi.org/10.1371/journal.pone.0246756.t001

steady-state level when surface coverage level approaches its equilibrium state due to the additional of the 1,2-DAB on Co_3O_4/Yb_2O_3 NPs/binder/GCE electrode. The experimental results presented in Fig 5B show a linear plot with the homogeneous distribution. This suggests that the proposed 1,2-DAB sensor could be applied successfully to toxin levels in buffer medium. The response time is required as 10.4 sec by the Co_3O_4/Yb_2O_3NPs/binder/GCE sensor probe based chemical sensing as shown in previously presented Fig 4C to reach steady-state response. Thus, it is possible to record and preserve the data within 10.4 sec. The fabricated Co_3O_4/ Yb_2O_3NPs/binder/GCE sensor probe is found to be efficient in terms of DL and DLR selectively. Table 1 shows the comparison of chemical sensors fabricated with various nanostructured metals by electrochemical methods.

Real sample analysis

The newly developed Co_3O_4/Yb_2O_3 NPs/binder/GCE based chemical sensor was justified for its applicability within the practical field through employing it in detecting 1,2-DAB with verities of real samples collected from the various sources. To confirm its wide range of applicability, the tested real samples were collected from different sources including extracts from PC baby-bottles, PC water bottles, PVC-made food packing bags, and so on. The collected samples are initially filtered. Finally, the samples are used to detect by fabricated Co_3O_4/Yb_2O_3 NPs/ binder/GCE sensor probe using an electrochemical method in room conditions. The obtained results as presented in Table 2, are found to be quite satisfactory and acceptable.

Conclusions

Finally, nanoparticles of Co_3O_4/Yb_2O_3 were prepared hydrothermally and analyzed by various conventional methods, such as UV-vis, FTIR, FESEM, EDS, XRD and XPS. A selective chemical sensor probe was successfully prepared through depositing a very thin layer of Co_3O_4/ Yb_2O_3 NPs onto GCE. During deposition process, a drop of Nafion was added for improving its fabrication process to stick the powder NPs onto GCE surface. The fabricated sensor probe was then employed in detecting the target toxic 1,2-DAB in phosphate buffer system. The 1,2-DAB chemical sensor is exhibited satisfactory results for various analytical performing factors including detection limit, selectivity, linearity, response time, reproducibility,

Table 2. Measured concentrations of 1,2-DAB analytes for different real samples by an electrochemical method using Co_3O_4/Yb_2O_3 NPs/Nafion/GCE.

Real sample	Observed current (μA)				Average	Measured Conc. (μM)	%SD
	Reading 1	Reading 2	Reading 3	Reading 4			
Industrial effluents	1.59	1.61	1.62	1.64	1.615	0.0113	1.29
PC baby bottle	2.84	2.88	2.95	2.97	2.910	0.0206	2.08
PC water bottle	2.26	2.19	2.14	2.23	2.205	0.0156	2.36
Packing bag/PVC	2.37	2.46	2.50	2.61	2.485	0.0176	4.00

*SD–Standard deviation, μM–Micromole.

https://doi.org/10.1371/journal.pone.0246756.t002

repeatability, stability, and so on. The obtained sensitivity and LDR (linear dynamic range) are observed to be 5.6962 $\mu A\mu M^{-1}cm^{-2}$ and 0.1 pM—0.01 mM respectively. The DL (detection limit) is found to be 0.02 ± 0.001 pM at the point where the signal to noise ratio is 3. The test results are obtained from various real sample sources demonstrated that the fabricated sensor is highly reliable and suitable in detecting toxins by an electrochemical process on a broad scale. Thus, a sensor probe with binary doped nanostructure material is applied and useful for the safety of environmental and health care fields on a large scale.

Author Contributions

Conceptualization: Mohammed M. Rahman.

Data curation: Mohammed M. Rahman.

Investigation: Mohammed M. Rahman.

Methodology: Mohammed M. Rahman.

Writing – review & editing: Mohammed M. Rahman.

References

1. Gichner T, Stavreva DA, Van Breusegem F. O-Phenylenediamine-induced DNA damage and mutagenicity in tobacco seedlings is light-dependent. Genet. Toxicol. Environ. Mutagen. 2001; 495:117–125. https://doi.org/10.1016/s1383-5718(01)00204-2 PMID: 11448649

2. Li JH, Kuang DZ, Feng YL, Liu MQ. Voltammetric determination of ophenylenediamine in industrial wastewater by an electrode modified with nanocomposite film of TiO2/hydroxyapatite/MWCNT. Chin. J. Anal. Chem. 2011; 39:1864–1870. https://doi.org/10.3724/SP.J.1096.2011.01864

3. Matsumoto M, Suzuki M, Kano H, Aiso S, Yamazaki K, Fukushima S. Carcinogenicity of ortho-phenylenediamine dihydrochloride in rats and mice by two-year drinking water treatment. Arch. Toxicol. 2012; 86:791–804. https://doi.org/10.1007/s00204-012-0800-z PMID: 22270912

4. Li N, Gua Y, Gao M, Wang Z, Xiao D, Li Y, et al. Colorimetric determination of o-phenylenediamine in water samples based on the formation of silver nanoparticles as a colorimetric probe. Spectrochim. Acta, Part A 2015; 140:328–333. https://doi.org/10.1016/j.saa.2014.12.053 PMID: 25615678

5. Rastogi SC. A method for the analysis of intermediates of oxidative hair dyes in cosmetic products. J. Sep. Sci. 2001: 24: 173–178. https://doi.org/10.1002/1615-314(20010301)24:3<173::AID-JSSC173>3.0.CO;2-L

6. Zhou J, Xu H, Wan GH, Duan CF, Cui H. Enhancing and inhibiting effects of aromatic compounds on luminol-dimethylsulfoxide-OH (-) chemiluminescence and determination of intermediates in oxidative hair dyes by HPLC with chemiluminescence detection. Talanta 2004; 64:467–477. https://doi.org/10.1016/j.talanta.2004.03.015 PMID: 18969627

7. Wang SP, Huang TH. Separation and determination of aminophenols and phenylenediamines by liquid chromatography and micellar electrokinetic capillary chromatography. Anal. Chim. Acta. 2005; 534:207–214. https://doi.org/10.1016/j.aca.2004.11.038

8. Bilal S, Holze R. In situ UV–vis Spectro electrochemistry of poly (ophenylenediamine-co-m-toluidine). Electrochim. Acta 2007; 52:5346–5356. https://doi.org/10.1016/j.electacta.2007.02.034

9. Altun O, Akbas H, Dolen E. Kinetic spectrophotometric method for ophenylenediamine in the presence of gold (III). Spectrochim. Acta A 2007; 66:499–502. https://doi.org/10.1016/j.saa.2006.02.065 PMID: 16859972

10. Dong S, Chi SL, Zhang S, He P, Wang Q, Fang Y. Simultaneous determination of phenylenediamine isomers and dihydroxybenzene isomers in hair dyes by capillary zone electrophoresis coupled with amperometric detection, Anal. Bioanal. Chem. 2008; 391:653–659. https://doi.org/10.1007/s00216-008-2053-5 PMID: 18421447

11. Li N, Gu Y, Gao M, Wang Z, Xiao D, Li Y, et al. Colorimetric determination of o-phenylenediamine in water samples based on the formation of silver nanoparticles as a colorimetric probe. Spectrochim. Acta, Part A 2015; 140:328–333. https://doi.org/10.1016/j.saa.2014.12.053 PMID: 25615678

12. Ye W, Kou SF, Guo X, Xie F, Sun HY, Lu HT, et al. Controlled synthesis of bimetallic Pd–Rh nanoframes and nanoboxes with high catalytic performances. Nanoscale 2015; 7:9558–9562. https://doi.org/10.1039/c4nr06917j PMID: 25947355

13. Liu JB, Hu NX, Hou S, Wen T, Liu WQ, Zhu X, et al. Au@Pt core/shell nanorods with peroxidase- and ascorbate oxidase-like activities for improved detection of glucose. Sens. Actuators B 2012: 166–167:708–714. https://doi.org/10.1016/j.snb.2012.03.045

14. Chang YY, Xie SB, Chai YQ, Yuan YL, Yuan R. 3,4,9,10-Perylenetetracarboxylic acid/o-phenylenedia-mine nanomaterials as novel redox probes for electrochemical aptasensor systems based on an Fe3O4 magnetic bead as a nonenzymatic catalyst. Chem. Commun. 2015; 51:7657–7660. https://doi.org/10.1039/C5CC00684H PMID: 25848657

15. Li N, Yan Y, Xia BY, Wang TY, Wang X. Novel tungsten carbide nanorods: An intrinsic peroxidase mimetic with high activity and stability in aqueous and organic solvents. Biosens. Bioelectron. 2014; 54:521–527. https://doi.org/10.1016/j.bios.2013.11.040 PMID: 24325981

16. Sasikumar R, Ranganathan P, Chen SM, Rwei SP, Muthukrishnan. Electro-oxidative determination of aromatic amine (o-phenylenediamine) using organic-inorganic hybrid composite. J. Colloid Interface Sci. 2017; 504:149–157. https://doi.org/10.1016/j.jcis.2017.05.043 PMID: 28544916

17. Zhao C, Jiang Z, Mu R, Li Y. A novel sensor for dopamine based on the turn-on fluorescence of Fe-MIL-88 metal-organic frameworks–hydrogen peroxide–ophenylenediamine system. Talanta. 2016; 159:365–370. https://doi.org/10.1016/j.talanta.2016.06.043 PMID: 27474319

18. Cherginets VL, Rebrova TP, Rebrov AL, Ponomarenko TV, Yurchenko OI. On some regularities of magnesium oxide solubility in melts with different content of alkaline earth metal chlorides. J. Chem. Thermodynamics 2017; 113:1–5. https://doi.org/10.1016/j.jct.2017.05.034

19. Hussain MM, Rahman MM, Asiri AM, Awual MR. Non-enzymatic simultaneous detection of Lglutamic acid and uric acid using mesoporous Co3O4 nanosheets. RSC Adv. 2016; 6:80511–80521. https://doi.org/10.1039/c6ra12256f

20. Rahman MM, Khan SB, Faisal M, Rub MA, Al-Youbi AO, Asiri AM. Talanta 2012; 99:924–931. https://doi.org/10.1016/j.talanta.2012.07.060 PMID: 22967644

21. Rahman MM, Khan SB, Gruner G, Al-Ghamdid MS, Daouse MA, Asiri AM. Chloride ion sensors based on low-dimensional α-MnO2–Co3O4 nanoparticles fabricated glassy carbon electrodes by simple I–V technique. Electrochim. Acta. 2013; 103:143–150. https://doi.org/10.1016/j.electacta.2013.04.067

22. Hou J, Li Y, Mao M, Ren L, Zhao X. Tremendous Effect of the Morphology of Birnessite-Type Manga-nese Oxide Nanostructures on Catalytic Activity. ACS Appl. Mater. Interfaces 2014; 6:14981−14987. https://doi.org/10.1021/am5027743 PMID: 25140618

23. Luo X, Lee WT, Xing G, Bao N, Yonis A, Chu AD, et al. Ferromagnetic ordering in Mn-doped ZnO nano-particles. Nanoscale Res. Lett. 2014; 9:625. https://doi.org/10.1186/1556-276X-9-625 PMID: 25435834

24. Liu Y, Zhu G, Ge B, Zhou H, Yuan A, Shen X. Concave Co3O4 octahedral mesocrystal: polymer-medi-ated synthesis and sensing properties. CrystEngComm 2012; 14:6264–6270. https://doi.org/10.1039/C2CE25788B

25. Xu H, Hai Z, Diwu J, Zhang Q, Gao L, Cui D, et al. Synthesis and Microwave Absorption Properties of Core-Shell Structured Co3O4-PANI Nanocomposites. J. Nanomater. 2015; 845983. https://doi.org/10.1155/2015/845983

26. Patel VK, Saurav JR, Gangopadhyay K, Gangopadhyay S, Bhattacharya S. Combustion characteriza-tion and modeling of novel nanoenergetic composites of Co3O4/nAl. RSC Adv. 2015; 5:21471–21479. https://doi.org/10.1039/C4RA14751K

27. Huang X, Chen Z, Gao T, Huang Q, Niu F, Qin L, et al. Hydrogen Generation by Hydrolysis of an Al/Al2O3- Composite Powder After Heat Treatment. Energy Technol. 2013; 1:751–756. https://doi.org/10.1002/ente.201300129

28. Nidhin M, Sreeram KJ, Nair BU. Green synthesis of rock salt CoO nanoparticles for coating applications by complexation and surface passivation with starch. Chem. Eng. J. 2012; 185:352–357. https://doi.org/10.1016/j.cej.2011.11.104

29. Rahman MM, Jamal A, Khan SB, Faisal M. Fabrication of Highly Sensitive Ethanol Chemical Sensor Based on Sm-Doped Co3O4 Nanokernels by a Hydrothermal Method. J. Phys. Chem. C 2011; 115:9503–9510. https://doi.org/10.1021/jp202252j

30. Rahman MM, Gruner G, Al-Ghamdi MS, Daous MA, Khan SB, Asiri AM. Chemo-sensors development based on low-dimensional codoped Mn2O3-ZnO nanoparticles using flat-silver electrodes. Chem. Cent. J. 2013; 7:60. https://doi.org/10.1186/1752-153X-7-60 PMID: 23537000

31. Ramasamy R, Ramachandran K, Philip GG, Ramachandran R, Therese HA, kumar GG. Design and development of Co3O4/NiO composite nanofibers for the application of highly sensitive and selective non-enzymatic glucose sensors. RSC Adv. 2015; 5:76538–76547. https://doi.org/10.1039/C5RA11739A

32. Kumar S, Ojha AK. Ni, Co and Ni–Co codoping induced modification in shape, optical band gap and enhanced photocatalytic activity of CeO2 nanostructures for photodegradation of methylene blue dye under visible light irradiation. RSC Adv. 2016; 6: 8651–8660. https://doi.org/10.1039/C5RA14184B

33. Rahman MM, Alam MM, Asiri AM, Islam MA. Fabrication of selective chemical sensor with ternary ZnO/SnO2/Yb2O3 nanoparticles. Talanta 2017; 170:215–223. https://doi.org/10.1016/j.talanta.2017.04.017 PMID: 28501161

34. Rahman MM, Alam MM, Asiri AM, Islam MA. Ethanol sensor development based on ternary-doped metal oxides (CdO/ZnO/Yb2O3) nanosheets for environmental safety. RSC Adv. 2017; 7:22627–22639. https://doi.org/10.1039/C7RA01852E

35. Kang M, Zhou H. Facile Synthesis and Structural Characterization of Co3O4 Nanocubes. AIMS Mater. Sci. 2015; 2:16–27. https://doi.org/10.3934/matersci.2015.1.16

36. Yang X, Fan K, Zhu Y, Shen J, Jiang X, Zhao P, et al. Tailored graphene-encapsulated mesoporous Co3O4 composite microspheres for high-performance lithium ion batteries. J. Mater. Chem. 2012; 22:17278–17283. https://doi.org/10.1039/C2JM32571C

37. Xia H, Zhu D1, Luo Z, Yu Y, Shi X, Yuan G, et al. Hierarchically Structured Co3O4@Pt@ MnO2 Nano-wire Arrays for High-Performance Supercapacitors. Sci. Rep. 2013; 3:2978. https://doi.org/10.1038/srep02978 PMID: 24132040

38. Qian C, Zeng T, Liu H. Synthesis and down conversion Emission Property of Yb2O3:Eu3+ Nanosheets and Nanotubes. Adv. Condens. Matter Phys.2013; 519869. https://doi.org/10.1155/2013/519869

39. Shestakov MV, Tikhomirov VK, Kirilenko D, Kuznetsov AS, Chibotaru LF, Baranov AN, et al. Quantum cutting in Li (770 nm) and Yb (1000 nm) co-dopant emission bands by energy transfer from the ZnO nano-crystalline host. Optics Express 2011; 19:15955. https://doi.org/10.1364/OE.19.015955 PMID: 21934959

40. Jenkins R, Snyder RL. John Wiley & Sons 1994; 138:750–950.

41. Celebioglu A, Vempati S, Ozgit-Akgun C, Biyikliab N, Uyar T. Water-soluble non-polymeric electrospun cyclodextrin nanofiber template for the synthesis of metal oxide tubes by atomic layer deposition. RSC Adv. 2014; 4:61698–61705. https://doi.org/10.1039/C4RA12073F

42. Tan Y, Gao Q, Yang C, Yang K, Tian W, Zhu L, One-dimensional porous nanofibers of Co3O4 on the carbon matrix from human hair with superior lithium ion storage performance. Sci. Rep. 2015; 5:12382. https://doi.org/10.1038/srep12382 PMID: 26201874

43. Alevli M, Ozgit C, Donmez I, Biyikli N. The influence of N2/H2 and ammonia N source materials on optical and structural properties of AlN films grown by plasma enhanced atomic layer deposition. J. Cryst. Growth 2011; 335:51–57. https://doi.org/10.1016/j.jcrysgro.2011.09.003

44. Cui J, Zhang X, Tong L, Luo J, Wang Y, Zhang Y, et al. A facile synthesis of mesoporous Co3O4/CeO2 hybrid nanowire arrays for high performance supercapacitors. J. Mater. Chem. A 2015; 3:10425–10431. https://doi.org/10.1039/C5TA00860C

45. Ye Y, Kuai L, Geng B. A template-free route to a Fe3O4–Co3O4 yolk–shell nanostructure as a noble-metal free electrocatalyst for ORR in alkaline media. J. Mater. Chem. 2012; 22:19132–19138. https://doi.org/10.1039/C2JM33893A

46. Xia H, Zhu D, Luo Z, Yu Y, Shi X, Yuan J, et al. Hierarchically Structured Co3O4@Pt@ MnO2 Nanowire Arrays for High-Performance Supercapacitors. Sci. Rep. 2013; 3:2978. https://doi.org/10.1038/srep02978 PMID: 24132040

47. Edla R, Gupta S, Patel N, Bazzanella N, Fernandes R, Kothari DC, et al. Enhanced H2 production from hydrolysis of sodium borohydride using Co3O4 nanoparticles assembled coatings prepared by pulsed laser deposition. Appl. Catal., A 2016; 515:1–9. https://doi.org/10.1016/j.apcata.2016.01.031

48. Shang C, Dong S, Hu P, Guan J, Xiao D, Chen X, et al. Compatible interface design of CoO-based Li-O2 battery cathodes with Long-cycling stability. Sci. Rep. 2015; 5:8335. https://doi.org/10.1038/srep08335 PMID: 25720845

49. Jeong S, Park S, Cho J. High-Performance, Layered, 3D-LiCoO 2 Cathodes with a Nanoscale Co3O4 Coating via Chemical Etching. Adv. Energy Mater. 2011; 1:368–372. https://doi.org/10.1002/aenm.201100029

50. Dang L, Zhang G, Kan K, Lin Y, Bai F, Jing L, et al. Hetero-structured Co3O4/PEI–CNTs composite: fabrication, characterization and CO gas sensors at room temperature. J. Mater. Chem. A 2014; 2:4558–4565. https://doi.org/10.1039/C3TA15019D

51. Zhao J, Liu Z, Qin Y, Hu W. Fabrication of Co3O4/graphene oxide composites using supercritical fluid and their catalytic application for the decomposition of ammonium perchlorate. CrystEngComm 2014; 16:2001–2008. https://doi.org/10.1039/C3CE41535J

52. He K, Luo Y, Yu R, Qi J, Sun X, Yang Y, et al. Influence of Yb2O3 on electrical and microstructural characteristics of CaCu3Ti4O12 ceramics. Mater. Res. Bull. 2015; 69:98–103. https://doi.org/10.1016/j.materresbull.2014.11.054

53. Wang S, Lou F, Yu C, Zhou Q, Wang M, Feng S, et al. Influence of Al3+ and P5+ ion contents on the valence state of Yb3+ ions and the dispersion effect of Al3+ and P5+ ions on Yb3+ ions in silica glass. J. Mater. Chem. C 2014; 2:4406–4414. https://doi.org/10.1039/C3TC32576H

54. Rivera-López F, Pérez M. X-ray photoelectron spectroscopy: surface and depth profiling studies of glasses doped with Nd and Yb ions. Surf. Interface Anal. 2012; 44:927–930. https://doi.org/10.1002/sia.4921

55. Wu ZS, Ren W, Wen L, Gao L, Zhao J, Chen Z, et al. Graphene Anchored with Co3O4 Nanoparticles as Anode of Lithium Ion Batteries with Enhanced Reversible Capacity and Cyclic Performance. ACS Nano. 2010; 4:3187–3194. https://doi.org/10.1021/nn100740x PMID: 20455594

56. Yuan C, Yang L, Hou L, Shen L, Zhang F, Li D, et al. Large-scale Co3O4 nanoparticles growing on nickel sheets via a one-step strategy and their ultra-highly reversible redox reaction toward supercapacitors. J. Mater. Chem. 2011; 21:18183–18185. https://doi.org/10.1039/C1JM14173B

57. Rahman MM, Khan SB, Gruner G, Al-Ghamdi MS, Daous MA, Asiri AM. Chloride ion sensors based on low-dimensional -MnO2–Co3O4 nanoparticles fabricated glassy carbon electrodes by simple I–V technique. Electrochim. Acta 2013; 103:143–150. https://doi.org/10.1016/j.electacta.2013.04.067

58. Liu S, Lee SC, Patil U, Shackery I, Kang S, Zhang K, et al. J. Mater. Chem. A 2017; 5:1043–1049. https://doi.org/10.1039/C6TA07842G

59. Lee JS, Kim W, Cho S, Jun J, Choa KH, Jang J. Multidimensional hybrid conductive nanoplate-based aptasensor for platelet-derived growth factor detection. J. Mater. Chem. B 2016; 4:4447–4454. https://doi.org/10.1039/c6tb00726k PMID: 32263427

60. Leng X, Wei S, Jiang Z, Lian J, Wang G, Jiang Q. Carbon-Encapsulated Co3O4 Nanoparticles as Anode Materials with Super Lithium Storage Performance. Sci. Rep. 2015; 5:16629. https://doi.org/10.1038/srep16629 PMID: 26564802

61. Solf V, Iwasita T, Giordano MC. Electro-oxidation of O-phenylenediamine at platinum electrodes in acetonitrile solution. J. Electroanal. Chem. 1979; 105:169–179. https://doi.org/10.1016/S0022-0728(79)80348-4

62. Li Y, Wang F, Zhou G, Ni Y. Aniline degradation by electrocatalytic oxidation. Chemosphere 2003; 53:1229–1234. https://doi.org/10.1016/S0045-6535(03)00590-3 PMID: 14550354

63. Rahman MM, Alam MM, Asiri AM, Islam MA. 3,4-Diaminotoluene sensor development based on hydrothermally prepared MnCoxOy nanoparticles. Talanta 2018; 176:17–25. https://doi.org/10.1016/j.talanta.2017.07.093 PMID: 28917737

64. Alam MK, Rahman MM, Elzwawy A, Torati SR, Islam MS, Todo M, et al. Highly sensitive and selective detection of bisphenol A based on reduced graphene oxide decorated hydroxyapatite nanocomposites. Electrochim. Acta 2017; 241:353–361. https://doi.org/10.1016/j.electacta.2017.04.135

65. Rahman MM, Marwani HM, Algethami FK, Asiri AM. Comparative performance of hydrazine sensor development on various Mn$_3$O$_4$/Carbon-nanotubes, Mn3O4/Graphene-oxides, Mn3O4/Carbon-black nanocomposites. Mater. Express 2017; 7:169–179. https://doi.org/10.1166/mex.2017.1367

66. Hussain MM, Rahman MM, Asiri AM. Ultrasensitive and selective 4-Aminophenol chemical sensor development based on nickel oxide nanoparticles decorated carbon nanotube nanocomposites for green environment. J. Environ. Sci. 2017; 53:27–38. https://doi.org/10.1016/j.jes.2016.03.028 PMID: 28372752